Stability of the Pilot-Aircraft System in Maneuvering Flight

John R. Broussard* and Robert. F. Stengel†
The Analytic Sciences Corp., Reading, Mass.

A control-theoretic pilot model is incorporated in the analysis of pilot-aircraft motions during maneuvers. The pilot model is found to be of value for the definition of maneuvering flight stability boundaries, and it simulates pilot control actions during a representative task with reasonable fidelity. The model also is used to demonstrate the consequences of improperly adapted pilot response strategy. It is concluded that the pilot model presented here provides important capabilities for evaluation of flying qualities and for identifying proper piloting procedures during difficult maneuvers.

Introduction

HIGH-PERFORMANCE aircraft are susceptible to degraded flying qualities during maneuvering flight, and the effect of piloting actions plays a significant role in determining overall system stability. The pilot's task is made difficult by the need to adapt control strategies to varying aircraft dynamics, by potentially high work load, and by the physical and mental stresses associated with maintaining safe flight. Under such circumstances, improper piloting procedures can lead to loss of control. This paper presents results from a study of pilot-aircraft interactions during high angle-of-attack flight. A multi-input/multi-output control-theoretic human operator model is developed and applied to the stability problem. Effects of control mechanisms (e.g., conventional stick-surface linkages and aileron-rudder interconnect) and pilot adaptation to flight condition are described. Proper (i.e., stabilizing) control actions for maneuvering flight are illustrated, and an example of pilot-induced oscillation (PIO) due to pilot nonadaptivity is demonstrated.

Control-Theoretic Pilot Model

The optimal control pilot model used for this analysis contains the following elements: an *estimator*, which processes the pilot's observations to provide an estimate of the aircraft state; a *controller*, which mechanizes the pilot's regulating functions and transmits the results to the neuromuscular dynamics; and a *neuromuscular model*, which represents the dynamics of the pilot's limbs. The block diagram of the pilot-aircraft system, shown in Fig. 1, is similar to earlier optimal control pilot-aircraft models.[1-4] The pure time delay that is commonly modeled in human observations[1] is replaced by a first-order Padé approximation, a substitution frequently made in analysis of human response using quasilinear human models.[5] The substitution is useful, because it allows the predictor equations in the pure-time-delay optimal-control model to be eliminated. The aircraft and pilot model then can be combined in a single linear, time-invariant equation, shown in by Eq. (6) in the appendix. This form is easier to simulate, and its stability and response characteristics are readily defined by eigenvalues and eigenvectors. The stability of the pilot model's estimation and control dynamics can be defined independently, i.e., the eigenvalues (or poles) of the pilot estimator are uncoupled from the closed-loop poles of the pilot controller-aircraft system [Eq. (6)]. Similarities between the pure-time-delay model and the model in Fig. 1 include identical numerical values for the pilot control strategy matrix C, the observation covariance matrix associated with $\Delta v_y(t)$, and the neuromotor noise covariance matrix associated with $\Delta v_u(t)$. Parameters of the pilot model are defined in the Appendix.

Two algorithms have been derived for generating the coefficients of the pilot model.[6] One solves the regulator Riccati equation and is shown in the appendix; the other solves the estimator Riccati equation. These algorithms are self-starting and are completely automated for computer implementation. Any number of controls can be used, and current results have been obtained with up to three concurrent pilot outputs (longitudinal stick, lateral stick, and rudder pedals). The pilot model for this analysis is supported by a fully coupled, linear, six-degree-of-freedom, aircraft simulation.[7] The pilot model longitudinal/lateral-directional modes are coupled or uncoupled depending on the coupling in the aircraft model that is used in computing the pilot model.

Investigations of pilot-aircraft instability using the control-theoretic pilot model fall into two categories: those in which the pilot fails to stabilize an unstable aircraft, and those in which the pilot destabilizes a stable aircraft. In the first case, the pilot's time delay, observation noise, neuromuscular time constants, and scanning factors are important parameters. Assuming the aircraft's linearized dynamics have one or more unstable eigenvalues, the analysis determines pilot parameters for which the optimal control model fails to exist. The optimal control model fails to exist when one of the model algorithms *diverges*, i.e., when it is impossible to obtain a steady-state solution to one of the Riccati equations.

The second category of pilot-aircraft instability is related to the pilot's ability to adapt to changing flight conditions. In

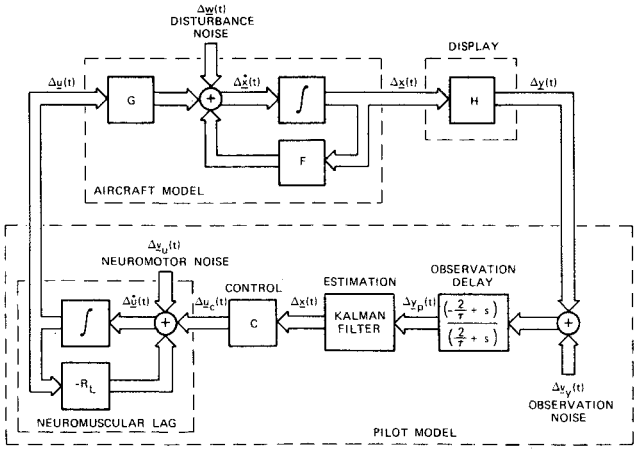

Fig. 1 Block diagram of the pilot-aircraft model.

Received June 30, 1976; revision received June 24, 1977.
Index categories: Handling Qualities, Stability and Control; Analytical and Numerical Methods; Human Factors.

*Member of the Technical Staff.

†Former Member of the Technical Staff; currently Associate Professor, Aerospace and Mechanical Sciences, Princeton University. Associate Fellow AIAA.

many situations, such as air combat and tracking, the pilot must maneuver the aircraft through widely varying flight conditions at high angles of attack, resulting in rapidly changing aircraft dynamics. These include such changes as the onset of adverse yaw due to ailerons, the migration of roll and spiral roots to unstable positions, and large variations in the natural frequency and damping of short period and Dutch roll modes. With the mean angle of attack α_0 changing (in some instances) faster than a degree per second, the pilot may not have the time to update his control strategy fast enough, and local instabilities can result. For example, pilot-induced oscillations (PIO) and departures can occur because a control strategy that is appropriate to one flight condition is destabilizing in another.

The control-theoretic pilot model can be used to analyze nonadapting pilot behavior in a straightforward manner. In the examples considered here, the pilot model's control strategy matrix C is first determined at a low-α_0 flight condition. This gain matrix is frozen and the aircraft's dynamics are allowed to change. The stability of the pilot-aircraft system is determined by its eigenvalues. The Kalman filter dynamics are assumed to be adapted and stable, as the subject of our study is the effect of fixed *control* strategy on closed-loop stability; thus, the Kalman filter only affects the simulation transient of the nonadapted pilot model and does not affect its stability.

Effects of Flight Conditions on Pilot-Aircraft Stability

The *open-loop* stability limits of the reference aircraft are shown in Fig. 2. The primary instabilities are an unstable Dutch roll mode in a band centered near $\alpha_0 = 20$ deg and unstable roll/spiral combination in a band near $\alpha_0 = 30$ deg.

The pilot's control outputs can include lateral stick for roll control, longitudinal stick for pitch control, and pedals for yaw control. When the aileron-rudder interconnect (ARI) system is engaged, the lateral stick commands to aileron are phased out as α_0 increases beyond 10 deg, and lateral stick-to-rudder commands are phased in. Above $\alpha_0 = 30$ deg, the lateral stick controls rudder only. The purpose of the ARI is to reduce adverse yaw effects due to aileron at high α_0, allowing the pilot to use low-α_0 strategies at high angle of attack.

The next three figures show simulations of the *adapted* linear-time-invariant control-theoretic model. In all cases, the disturbance and noise inputs are suppressed, and the model starts with a 10-deg heading error, which is to be nulled by the

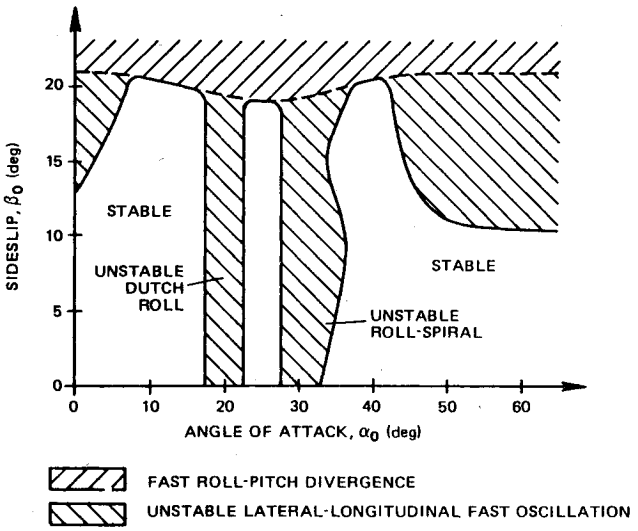

Fig. 2 Open-loop stability limits of the reference aircraft.

pilot model. Figure 3 shows piloting procedure at low-α_0 flight conditions using lateral stick alone and lateral stick plus rudder pedal. The figures illustrate that the modeled control patterns are very similar to the normal operating procedures of a human pilot. Initially, negative lateral stick movement rolls the aircraft and starts the heading change; this is followed by positive stick deflection to null roll rate and to zero roll angle at the new heading. The figure also demonstrates how the pilot can quicken lateral response by coordinated control of stick and pedals.

At higher angles of attack, adapted pilot model behavior with and without the ARI can be determined. Figure 4 shows such behavior at $\alpha_0 = 30$ deg, $\beta_0 = 0$ deg for control with lateral stick alone. When the ARI is on, as in Fig. 4a, the pilot model uses normal low-α_0 procedure to null the yaw angle, i.e., negative lateral stick to roll negatively. The ARI achieves its purpose, in terms of maintaining the same piloting procedure at high- and low-α_0 for lateral stick control. When the ARI is off, as in Fig. 4b, the pilot model must use a stick deflection that is opposite to the normal movement to null the yaw angle. This counter-intuitive control motion uses the adverse yaw of the lateral control surfaces to bank and turn the aircraft.

Figure 5 shows adapted pilot model behavior at high-α_0 for combined control with lateral stick and pedals. A comparison

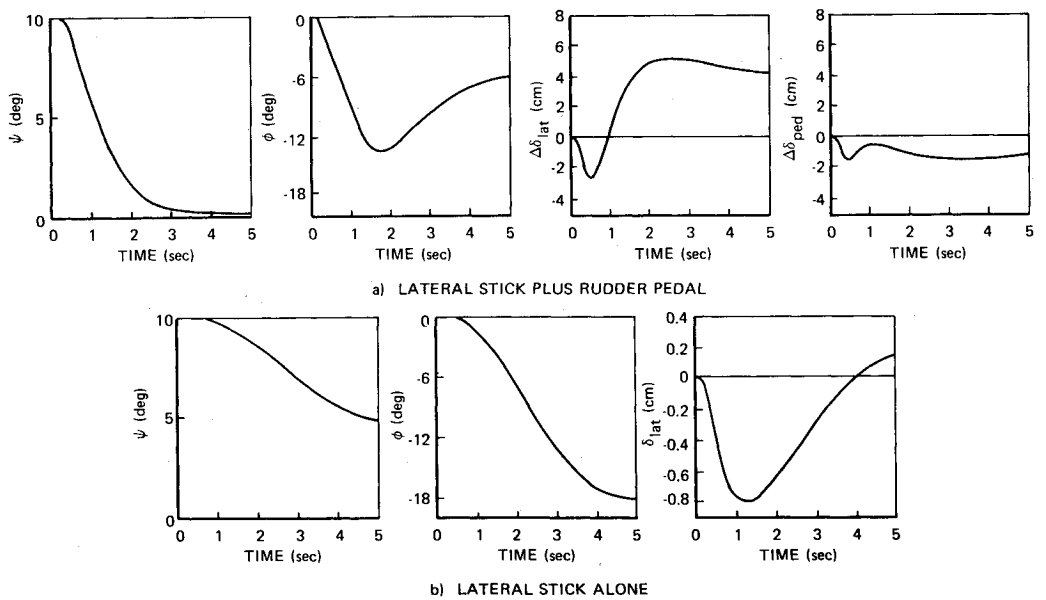

Fig. 3 Adapted piloting procedures at $\alpha_0 = 10$ deg.

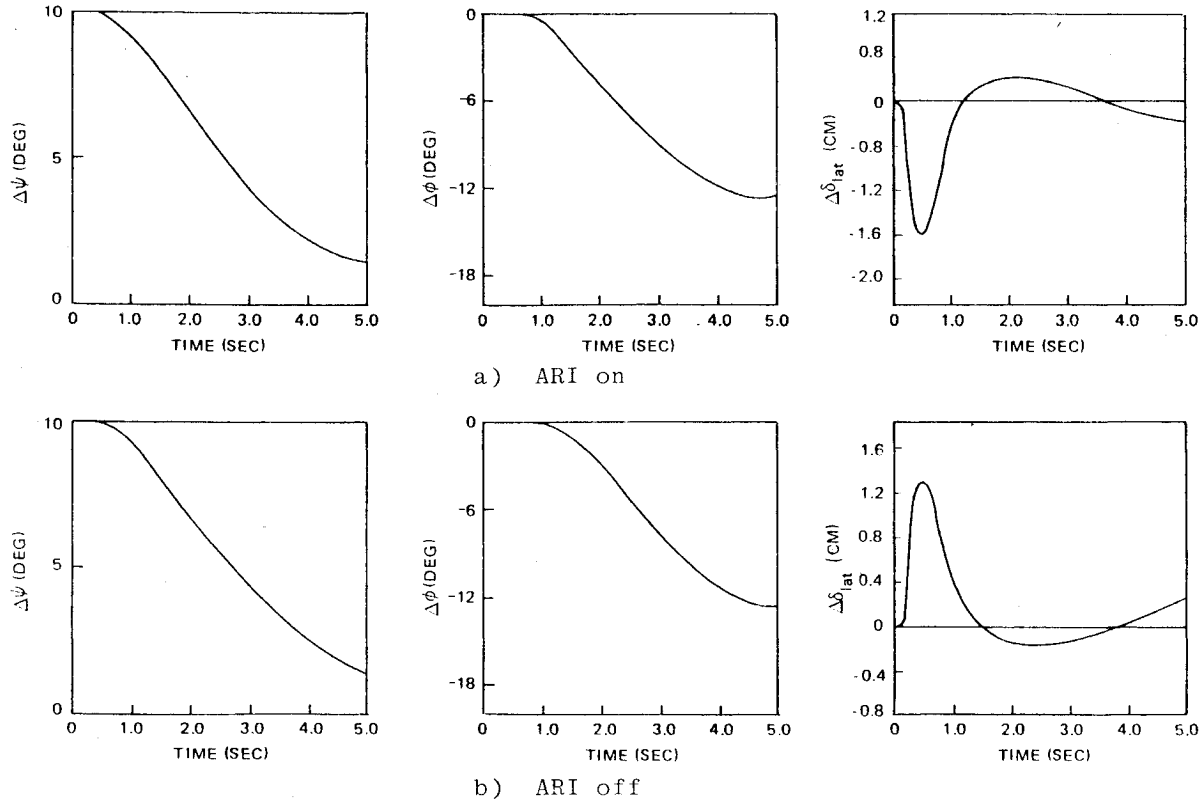

Fig. 4 Adapted lateral stick-alone piloting procedure at $\alpha_0 = 30$ deg.

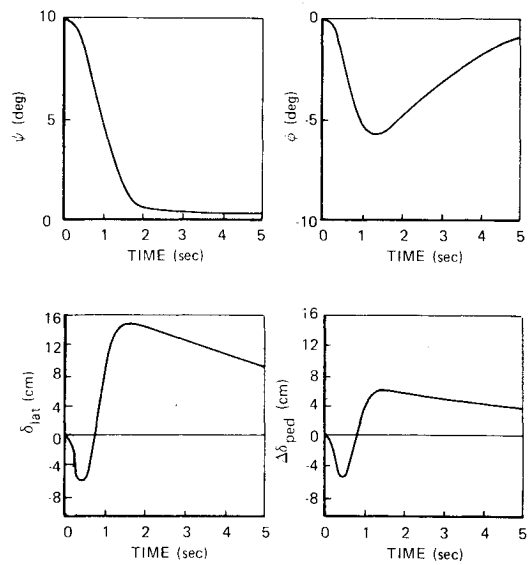

Fig. 5 Adapted lateral stick and pedal piloting procedure at $\alpha_0 = 30$ deg (ARI off).

with Fig. 3a shows that the lateral stick movements are similar, as are the initial pedal movements; however, the final pedal positions are opposite in sign. The positive pedal position in Fig. 5 is counteracting the adverse yaw caused by positive lateral stick at high α_0.

Nonadapted piloting effects on pilot-aircraft stability regions can be presented in the aircraft's $\alpha_0 - \beta_0$ plane. The regions of instability are determined, as previously mentioned, by fixing pilot control strategy C and determining eigenvalues of the closed-loop system [Eq. (6)]. Figure 6 shows the stability regions for three-control piloting procedures, and Fig. 7 shows stability regions under the assumption that the pilot does not use pedal control. In all cases, the pilot model is adapted to $\alpha_0 = 10$ deg and $\beta_0 = 0$ deg (denoted by ⊗ in the figures). This adaptation point was chosen arbitrarily; however, later results have shown that the stability boundaries are not particularly sensitive to the precise point of adaptation (as long as it is at a representative low-α_0 flight condition). The instabilities of the longitudinal modes (phugoid and short period) are the same in both cases, since the ARI does not affect longitudinal control. From Fig. 3a and 4b, it is evident that if the pilot model does not adapt, at some point the combination of adverse yaw and low-α_0 piloting procedure will lead to an instability. In Fig. 7a this occurs at $\alpha_0 \simeq 17$ deg, and the incorrect procedure is characterized by an unstable (closed-loop) spiral mode. When three controls are used with the ARI off, the instability due to incorrect procedures does not occur until $\alpha_0 \simeq 26$ deg, as shown in Fig. 6a. Figures 6b and 7b indicate that the ARI eliminates the spiral instability seen in Figs. 6a and 7a, but it introduces an unstable Dutch roll mode. In the stick-alone case, the instability occurs in bands centered on 20- and 32-deg angle of attack. Limited manned simulation results tend to confirm the closed-loop stability boundaries shown here.

Simulations of nonadapted procedure are readily obtained using the control-theoretic model, and these are shown in Figs. 8 and 9. Figure 8a shows the unstable Dutch roll mode with ARI engaged, of which only one cycle is evident. Note that negative lateral stick deflection causes the correct initial yaw response, but the pilot model's stick movement does not compensate fast enough. Figure 8b shows the unstable spiral mode response with ARI off, where negative lateral stick yaws the aircraft positively. The mismatched pilot model neglects the adverse yaw effect, responding to improper control response by even greater improper control. The simulation in Fig. 9a is stable for three controls with the ARI on. A comparison of Fig. 9a with Fig. 3a shows that the pilot model successfully uses the same strategy in both cases, but the 10-deg strategy provides too little damping at $\alpha_0 = 30$ deg. Figure 9b shows the unstable spiral mode for three controls with the ARI off. The initial direction in yaw angle is correct, but sluggishness in control movement, particularly in pedal, causes the instability.

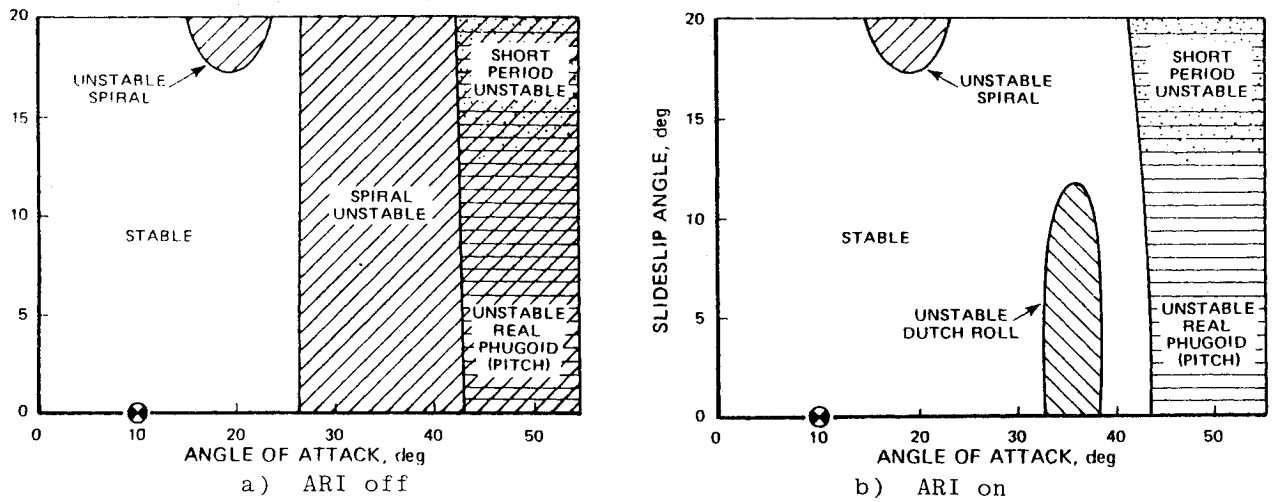

Fig. 6 Stability boundaries for 3-control piloting procedures.

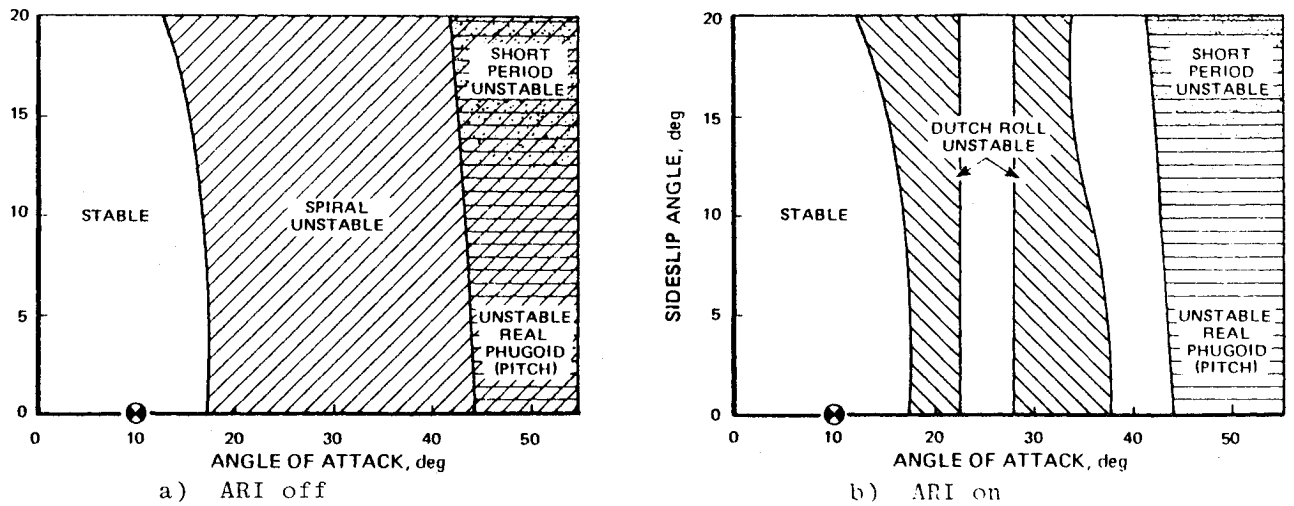

Fig. 7 Stability boundaries for 2-control piloting procedures.

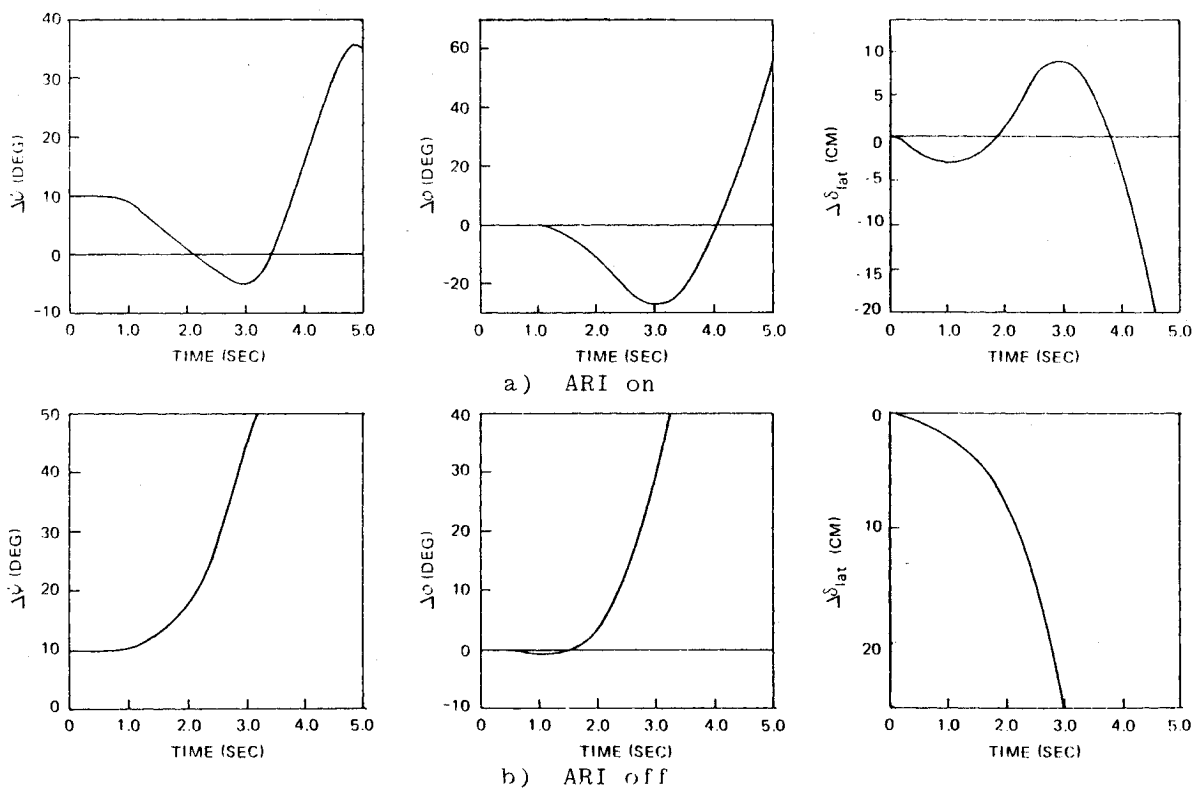

Fig. 8 Use of low-α_0 piloting procedure in high-α_0 flight with lateral stick alone. Pilot is adapted to $\alpha_0 = 10$ deg; aircraft is at $\alpha_0 = 30$ deg.

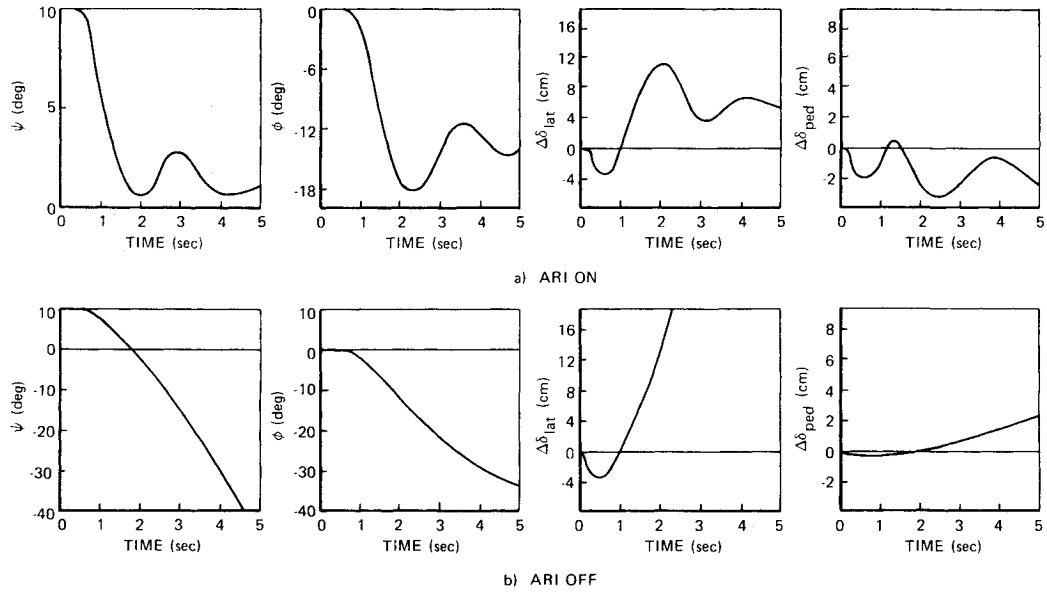

Fig. 9 Use of low-α_0 piloting procedure in high-α_0 flight with lateral stick plus foot pedals.

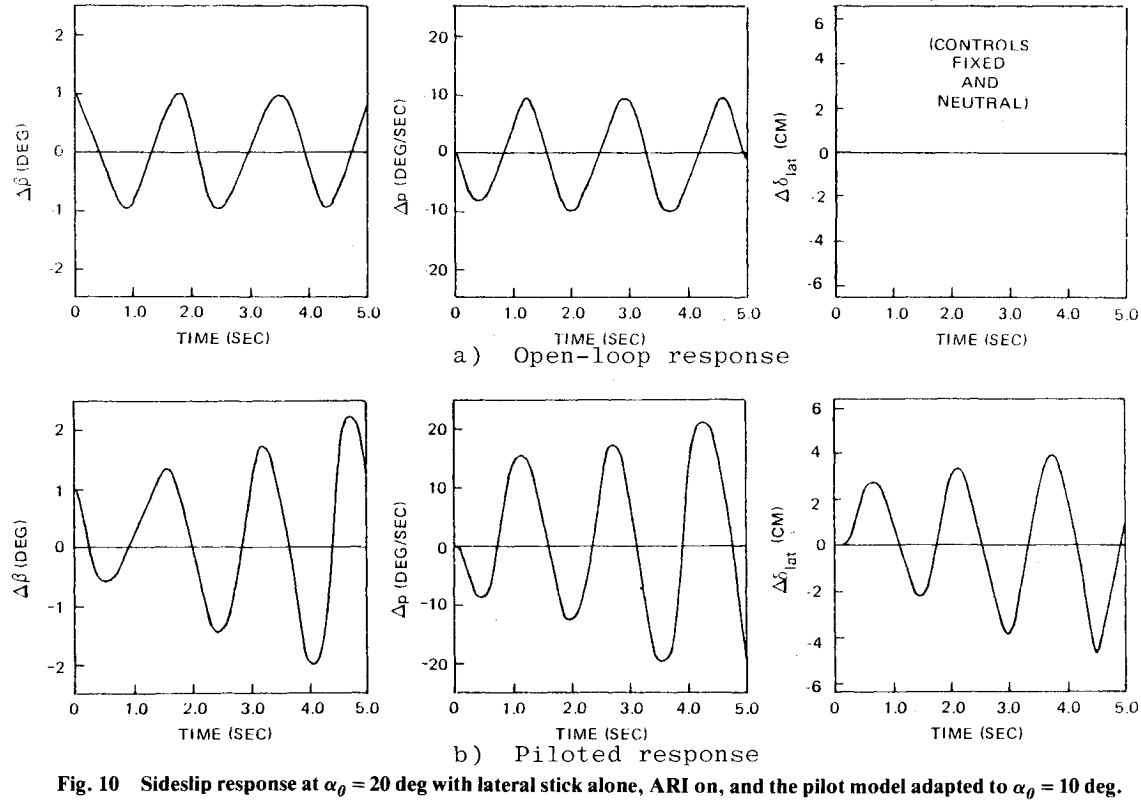

Fig. 10 Sideslip response at $\alpha_0 = 20$ deg with lateral stick alone, ARI on, and the pilot model adapted to $\alpha_0 = 10$ deg.

A direct indication of the destabilizing influence that a nonadapted pilot could have and that could lead to pilot-induced oscillations is illustrated in Fig. 10. Figure 10a shows the natural rolling motion of this aircraft at $\alpha_0 = 20$ deg, which is a consequence of a slightly unstable Dutch roll mode. In Fig. 10b, the ARI is on, the pilot model is adapted to $\alpha_0 = 10$ deg flight, and there is an initial sideslip perturbation ($\Delta\beta$) of 1 deg. If the pilot uses the low-α_0 learned response to attempt to null $\Delta\beta$ and Δp, he may inadvertently "pump" energy into the growing $\Delta\beta$ oscillation through the aileron's adverse yaw. The result is a pilot-induced diverging oscillation whose characteristics would normally be associated with *wing rock*. The highly oscillatory nature of the control actions presumably is the result of limitations on the control rates that the pilot model is able to use.

Conclusion

This paper has illustrated several ways in which a control-theoretic pilot model can be useful for examining the stability of the pilot-aircraft system. This system can be unstable for one of two reasons: either the aircraft itself is unstable and the pilot is incapable of providing stabilizing control actions, or the pilot can destabilize an otherwise stable aircraft by inappropriate control actions. The latter case can result when the pilot does not adapt to changing flight conditions, applying control strategies that are suitable for one flight condition in a dynamically dissimilar situation. Although not detailed in this paper, the stability boundaries and simulated time histories established with the nonadapted pilot model are compatible with experimental results obtained from manned simulation and flight test.

An inverse interpretation of the results obtained with the adapted pilot model is that they specify what the pilot *must* do in a given dynamic condition to achieve well-behaved, stable aircraft response. Given the accepted physiologic parameters contained in the design equations, the model illustrates what the well-motivated pilot can do to null flight path errors with available control effectors; hence, it identifies logical cues for compensatory control, and it depicts control deflection histories that can be learned as adjuncts to precognitive control. It is concluded that the control-theoretic pilot model is a valuable tool for further analysis of aircraft handling qualities and for understanding the piloting skills necessary for maneuvering flight.

Appendix

Mathematical Model

Small perturbations in the aircraft motion are approximated by the linear, time-invariant system

$$\Delta\dot{x}(t) = F\Delta x(t) + G\Delta u(t) + \Delta w(t) \tag{1}$$

where $\Delta x(t)$ represents the perturbation motion, $\Delta w(t)$ represents disturbance noise, and $\Delta u(t)$ is the pilot's compensatory control. The observations of the pilot are assumed to be

$$\Delta y(t) = H\Delta x(t-\tau) + D\Delta u(t-\tau) + \Delta v_y(t-\tau) \tag{2}$$

where τ is the pilot time delay and $\Delta v_y(t)$ represents pilot observation noise. The pilot is assumed to choose $\Delta u(t)$, when behaving optimally, by minimizing an infinite-time quadratic cost functional. This produces the control law

$$\Delta\dot{u}(t) = -R_L\Delta u(t) + C\Delta\hat{x}(t) + \Delta v_u(t) \tag{3}$$

where Δv_u represents pilot neuromotor noise. The matrix C is the pilot's feedback control strategy and the matrix R_L has the form

$$R_L = \begin{bmatrix} \frac{1}{\tau_{n_1}} & 0 & 0 \\ 0 & \frac{1}{\tau_{n_2}} & 0 \\ 0 & 0 & \frac{1}{\tau_{n_3}} \end{bmatrix} \tag{4}$$

where the scalars τ_{n_i} are neuromotor time constants of human limbs. The vector $\Delta\hat{x}(t)$ represents the pilot's estimate of the aircraft states based on observing $\Delta y(t)$. The pilot model observations can be restructured by using the Padé approximation to $e^{-\tau s}$ in Eq. (2) as follows:

$$\Delta y(s) = \frac{2-\tau s}{2+\tau s}\left[H\Delta x(s) + D\Delta u(s) + \Delta v_y(s)\right] \tag{5}$$

Using Eqs. (1), (3), and (5), the closed-loop pilot aircraft system can be shown to be

$$\begin{bmatrix} \Delta\dot{x}(t) \\ \Delta\dot{u}(t) \\ \Delta\dot{z}(t) \\ \hline \Delta\dot{\hat{x}}(t) \\ \Delta\dot{\hat{u}}(t) \\ \Delta\dot{\hat{z}}(t) \end{bmatrix} = \left[\begin{array}{ccc:ccc} F & G & 0 & 0 & 0 & 0 \\ C & -R_L & 0 & C & 0 & 0 \\ H & D & \left[-\frac{2}{\tau}I\right] & 0 & 0 & 0 \\ \hline & & & & & \\ & 0 & & & F_f & \end{array}\right] \times \begin{bmatrix} \Delta x(t) \\ \Delta u(t) \\ \Delta z(t) \\ \hline \Delta\hat{x}(t) \\ \Delta\hat{u}(t) \\ \Delta\hat{z}(t) \end{bmatrix} + \left[\begin{array}{cc:c} I & 0 & \\ & & \\ \hline -I & K & \end{array}\right] \begin{bmatrix} \Delta w(t) \\ \Delta v_u(t) \\ \Delta v_y(t) \\ \hline -\Delta v_y(t) \end{bmatrix} \tag{6}$$

In Eq. (6), F_f is the closed-loop system matrix used by the estimator, and K is the Kalman filter gain. Nonzero values of disturbance and noise covariances are used to define estimator gains; however, these effects are suppressed for clarity in this paper's time histories. The states $\Delta x(t)$, $\Delta u(t)$, and $\Delta z(t)$ are the estimation errors. The states $\Delta z(t)$ are used to represent the delay after the Padé approximation. The matrix C does not change.

Assumptions

The pilot model's outputs drive the aircraft through the matrix G, which is adjusted to account for the ARI being on or off. The pilot is assumed to observe only the perturbation angles and angular rates of the aircraft. The pilot's observation noise-to-signal ratio is set at 0.025π to account for scanning,[3] and the aircraft is assumed to be forced by a turbulence model.[4] The neuromotor noise-to-signal ratio is set at 0.0003π. The pilot is assumed to have a time delay of 0.2 sec and a neuromuscular time constant of 0.1 sec for each limb.

The state and control weighting matrix Q is adjusted until a reasonable set of mean-square covariance values of the aircraft states are obtained.[6] Present results indicate that closed-loop eigenvalues of the pilot model regulator may be relatively insensitive to Q, as the adjustment of the control-rate weighting to maintain R_L in the optimal control pilot model appears to have a strong effect on *relative* weightings of states and controls. The control-rate weighting matrix R is found using the following algorithm.

Pilot Model Regulator Algoritm

The pilot model regulator Riccati equation is given by

$$0 = SF' + F'^{T}S + Q - SG'R^{-1}G'^{T}S \tag{7}$$

where R weights the control rate, and Q weights the states and controls in a quadratic cost functional. The following substitutions are made:

$$F' = \left[\begin{array}{c:c} F & G \\ \hline 0 & 0 \end{array}\right] \tag{8}$$

$$G' = \begin{bmatrix} 0 \\ \hline I \end{bmatrix} \tag{9}$$

$$S' = \left[\begin{array}{c:c} S_{11} & S_{12} \\ \hline S_{21} & S_{22} \end{array}\right] \tag{10}$$

$$R_L = R^{-1}S_{22} \tag{11}$$

Solving for R in Eq. (11) and using Eq. (9), Eq. (7) can be restated as follows:

$$0 = SF' + F'^{T}S + Q - SG'(G'^{T}SG'R_L{}^{-1})^{-1}G'^{T}S \tag{12}$$

If an initial S can be found in the contraction mapping convergence sphere of Eq. (12), repeated substitution converges to the solution of Eq. (12). The following iterative

scheme strives to achieve the solution:

1) Choose a positive definite R_0 and solve for S_0 in

$$0 = S_0F' + F'^{T}S_0 + Q - S_0G'R_0^{-1}G'^{T}S_0$$

2) Continue with the following until some convergence criterion is satisfied (unless R_1 does not become greater than R_2):

$$R_K = G'^{T}S_{K-1}G'R_L^{-1}$$

$$C_K = R_K^{-1}G'^{T}S_{K-1} \qquad (K = 1,2,\ldots)$$

$$F'_K = F' - G'C_K$$

$$0 = S_KF'_K + F'^{T}_KS_K + Q + C_K^{T}R_KC_K$$

3) If R_1 does not become greater than R_2, increase R_0 and go back to step 1.

4) If R_0 exceeds a maximum acceptable value, either R_0 is larger than the stopping value or no solution exists. The philosophy is to choose a stabilizing S_0 that is greater than the solution S. Reference 9 provides a similar algorithm in which $R_L = \sigma I$, where σ is a scalar; R is therefore symmetric [Eq. (11)]. The algorithm developed here requires only that R_L be an appropriate positive definite matrix; hence, R may be asymmetric.

Acknowledgment

This work was conducted under Contract No. N00014-75-C-9432 for the Office of Naval Research, Department of the Navy. Presented at the 12th Annual Conference on Manual Control, Urbana, Ill., May 25-27, 1976.

References

[1] Kleinman, D. L., Baron, S., and Levison, W. H., "A Control Theoretic Approach to Manned-Vehicle Systems Analysis," *IEEE Transactions on Automatic Control*, Vol. AC-16, Dec. 1971, pp. 824-832.

[2] Kleinman, D. L. and Baron, S., "Manned Vehicle Systems Analysis by Means of Modern Control Theory," Bolt, Beranek and Newman, Cambridge, Mass., BBN Rept. 1967, June 1970.

[3] Baron, S. and Levison, W. H., "An Optimal Control Methodology for Analyzing the Effects of Display Parameters on Performance and Workload in Manual Flight Control," *IEEE Transactions on Systems, Man, and Cybernetics*, Vol. SMC-5, July 1975, pp. 423-430.

[4] Baron, S. and Levison, W. H., "A Manual Control Theory Analysis of Vertical Situation Displays for STOL Aircraft," NASA CR-114640, April 1973.

[5] Kugel, D. L., "Determination of In-Flight Pilot Parameters Using a Newton-Raphson Minimization Technique," *Proceedings of the 10th Annual Conference on Manual Control*, Wright-Patterson AFB, April 9-11, 1974.

[6] Stengel, R. F., Taylor, J. H., Broussard, J. R., and Berry, P. W., "High-Angle of Attack Stability and Control," The Analytic Sciences Corp., Reading, Mass., ONR-CR215-237-1, April 1976.

[7] Stengel, R. F. and Berry, P. W., "Stability and Control of Maneuvering High-Performance Aircraft," NASA CR-2788, April 1977.

[8] Kleinman, D. L., "On an Iterative Technique for Riccati Equation Computations," *IEEE Transactions on Automatic Control*, Vol. AC-13, Feb. 1968, pp. 114-115.

[9] Kleinman, D. L., "Numerical Solution of the State Dependent Noise Problem," *IEEE Transactions on Automatic Control*, Vol. AC-21, June 1976, pp. 419-420.